Available online at www.sciencedirect.com

SciVerse ScienceDirect

Ceramics International 39 (2013) 3235–3242

CERAMICS INTERNATIONAL

www.elsevier.com/locate/ceramint

Structure and magnetic properties of $Zn_{1-x}In_xFe_2O_4$ and $ZnY_xFe_{2-x}O_4$ nanoparticles prepared by coprecipitation

Marija Milanović[a,*], Evagelia G. Moshopoulou[b], Dimosthenis Stamopoulos[b], Eamonn Devlin[b], Konstantinos P. Giannakopoulos[b,c], Athanassios G. Kontos[d], Kostas Eleftheriadis[e], Maria I. Gini[e], Ljubica M. Nikolić[a]

[a]*Department of Materials Engineering, Faculty of Technology, University of Novi Sad, Bulevar cara Lazara 1, 21000 Novi Sad, Serbia*
[b]*Institute of Materials Science, NCSR "Demokritos", 15310 Agia Paraskevi, Athens, Greece*
[c]*Institute of Microelectronics, NCSR "Demokritos", 15310 Agia Paraskevi, Athens, Greece*
[d]*Institute of Physical Chemistry, NCSR "Demokritos", 15310 Agia Paraskevi, Athens, Greece*
[e]*Institute of Nuclear Technology & Radiation Protection, NCSR "Demokritos", 15310 Agia Paraskevi, Athens, Greece*

Received 27 August 2012; received in revised form 28 September 2012; accepted 2 October 2012
Available online 9 October 2012

Abstract

Zinc ferrites, $ZnFe_2O_4$ and zinc ferrite nanoparticles substituted with indium and yttrium, $Zn_{1-x}In_xFe_2O_4$ and $ZnY_xFe_{2-x}O_4$ ($0 \le x \le 0.3$), were synthesized by co-precipitation method. We have investigated the effect of composition on the cation distribution in the spinel structure, and on the magnetic properties with a view to obtain magnetic ceramics with improved properties compared to their bulk counter parts. The results of X–ray diffraction (XRD) and transmission electron microscopy (TEM) confirmed the nanoscale dimensions and spinel structure of the samples. The estimated crystallite size lies within the range 4–10 nm. Additional experiments had been conducted using a scanning mobility particle sizer spectrometer (SMPS) in order to measure the number size distribution of the nanoparticles. Mössbauer spectroscopy was used to investigate the cation distribution between the tetrahedral and octahedral sites and the formation of the partially inverse spinel. The study of the magnetic properties showed that the hysteresis loops do not saturate even in the presence of high magnetic fields, confirming the superparamagnetic single domain nature of the samples. The particle size and composition variations (e.g. addition of yttrium and indium) cause significant structural rearrangements which affect the magnetic behavior of these materials.

Keywords: A. Powders: chemical preparation; C. Magnetic properties; D. Spinels

1. Introduction

Zinc ferrites are important technological materials widely used as photo catalysts, as regenerable absorbent materials for hot gas desulphurization, as the magnetic cores in RF devices, in sensors, in magnetic resonance imaging, etc. [1–3]. Especially nanocrystalline zinc ferrites have attracted a significant scientific interest because of their unique properties such as chemical and thermal stability and interesting magnetic properties strongly governed by the particle size. Zinc ferrite adopts a spinel structure with oxygen ions forming a cubic close packed structure with the metal ions occupying 1/8 of the tetrahedral (A) and 1/2 of the octahedral (B) interstitial sites [4].

Bulk zinc ferrite has a normal spinel structure with the diamagnetic Zn^{2+} ions in the tetrahedral sites and magnetic Fe^{3+} ions in the octahedral sites. Due to antiferromagnetic superexchange interactions between octahedrally coordinated Fe^{3+} ions, bulk zinc ferrite is antiferromagnetic at $T_N = 10$ K. However, scaling to nanometer sizes the magnetic structure of zinc ferrites changes significantly with the redistribution of iron and zinc cations into octahedral and tetrahedral sites. As a result, nanocrystalline zinc ferrite shows ferrimagnetic behavior. It has been demonstrated that the properties of zinc ferrites are

*Corresponding author. Tel.: +381 21 485 3750; fax: +381 21 450 413.
E-mail address: majam@uns.ac.rs (M. Milanović).

0272-8842/$ - see front matter © 2012 Elsevier Ltd and Techna Group S.r.l. All rights reserved.
http://dx.doi.org/10.1016/j.ceramint.2012.10.011

strongly influenced by the composition and microstructure and can be modified controllably by varying the particle size, the preparation method, the synthesis processing parameters, type and concentration of dopants etc. [1,3,5,6].

Magnetic dilution due to substitution of diamagnetic atoms gives rise to interesting magnetic features in spinel structure compounds. The addition of trivalent ions such as Nd^{3+}, Cr^{3+}, Y^{3+}, In^{3+} etc., influence the structural, electrical and magnetic properties of the nanocrystalline ferrites depending on the amount of the used cations [2,7–11]. We have already reported on the structural and electrical properties of yttrium and indium doped zinc ferrites [12,13]. High resistivities and low dielectric loss factors makes these ferrites particularly useful for high frequency applications. However, the magnetic properties of In^{3+} and Y^{3+} substituted nanocrystalline zinc ferrites prepared by co-precipitation technique have not been investigated in detail. In the light of lack investigations of indium and yttrium doped zinc ferrites, the present study reports the effect of doping on the parent spinel ferrite, aiming to obtain materials with high performance magnetic properties, such as saturation magnetization, coercivity, etc.

2. Experimental

2.1. Synthesis of nanoparticles

The co-precipitation method was used for the preparation of zinc ferrite–based materials. The chemical reagents used in the work are ferric nitrate ($Fe(NO_3)_3 \cdot 9H_2O$), zinc nitrate ($Zn(NO_3)_2 \cdot 6H_2O$), indium chloride ($InCl_3$), yttrium chloride (YCl_3) and sodium hydroxide (NaOH). All chemicals have analytical purity and were used without further purification. 0.2 M aqueous solutions of metal ions are prepared separately. In order to obtain $ZnFe_2O_4$ nanoparticles, 50 ml of Fe^{3+} aqueous solution and 25 ml of Zn^{2+} aqueous solution were mixed together. For the preparation of $Zn_{1-x}In_xFe_2O_4$ and $ZnY_xFe_{2-x}O_4$ ($x=0$, 0.15 and 0.3) nanoparticles, appropriate amounts of metal ions solutions were mixed together in the required stoichiometric ratio. These ferrite precursors were precipitated from the mixture by the gradual adding of 5 M NaOH at room temperature until the pH value reached 12. The co-precipitation reaction was carried out at 80 °C for 60 min under continuous stirring. The precipitates were separated from the slurry by centrifuging and washed with distilled water and absolute ethanol. The obtained powders were dried at 120 °C for 24 h and finally dry-milled in a mortar.

2.2. Characterization techniques

Conventional powder X-ray diffraction was carried out using a Siemens D500 diffractometer with CuKα radiation ($\lambda=0.1506$ nm) and a step size 0.03 °/15 s. The CellRef program was used to extract the lattice parameters assuming the cubic Fd3m space group. The average grain size (d_{XRD}) was estimated by the Scherrer equation using the FWHM of the (311) line [14]. The specific surface area of the as-synthesized nanopowders was measured by nitrogen adsorption according to the Brunauer–Emmett–Teller (BET) method using a Micrometrics, ASAP 2000 instrument. Average particle size (d_{BET}) was estimated from the specific surface area assuming a spherical shape. Number size distribution measurements were conducted using an atomizer aerosol generator (ATM 220/226 Topas GmbH) and a scanning mobility particle sizer spectrometer which exhibits very high size resolution. The aerosol, diluted with filtered air, entered a mixing chamber (total inner flow 1 l/min). A filtered secondary flow (10 l/min), forming a loop, also entered the mixing chamber. The secondary flow, before entered the chamber, passed through a container filled with silicon in order to be dried. The secondary flow causing the aerosol particles leaving the chamber to be of uniform size and dried (RH < 5%). The dried particles are passed through a neutralizer (Kr-85 radioactive source) in order to acquire a reproducible and known charge distribution. Then, the charged particles entered the SMPS, consisting of an electrostatic classifier (TSI 3080) and a condensation particle counter (CPC). First, the classifier separated the particles by size according to their electrical mobility. Then, particles which were size selected in the electrostatic classifier are passed to the CPC (CPC 3772, TSI) to measure the number concentration. High resolution transmission electron microscopy (HRTEM) and selected area electron diffraction (SAED) experiments were performed with a Philips CM20 TEM operating at 200 KV, equipped with an energy-dispersive X-ray spectroscopy probe (EDS). The ^{57}Fe Mössbauer spectra were recorded at 4.2 K on a conventional constant acceleration spectrometer with a ^{57}Co(Rh) source moving at room temperature (RT). The isomer shift values are quoted with respect to metallic iron at room temperature. Magnetization measurements were carried out using a Quantum Design SQUID magnetometer. Zero-field cooled (ZFC) and field cooled (FC) measurements were obtained in the temperature range $5 < T < 300$ K in an applied magnetic field of 100 Oe. Magnetization versus field measurements (hysteresis loops) were carried out at 5 K with fields ranging from −50 to 50 kOe.

3. Results and discussion

3.1. Structural properties and morphology

Fig. 1 shows the XRD patterns of the $Zn_{1-x}In_xFe_2O_4$ and $ZnY_xFe_{2-x}O_4$ nanoparticles ($x=0$, 0.15 and 0.3). All the as-synthesized powders are crystalline and their Bragg peaks can be indexed unambiguously assuming the spinel phase (JCPDS card 22-1012). The diffraction peaks of all samples are very broad indicating the small size of the particles formed at the rather low temperature of 80 °C. The average sizes of the nanoparticles calculated by the Scherrer formula are listed in Table 1. Interestingly, the influences of the dopants, Y^{3+} or In^{3+}, on the particle size are quite different. The evolution of the Bragg peak

broadening as a function of x for the indium and yttrium doped zinc ferrite nanoparticles implies that the crystallite size increases with yttrium content, but decreases with indium content. Evidence that this behavior stems indeed from the doping, comes from the observation that the diffraction peaks of the $Zn_{1-x}In_xFe_2O_4$ and $ZnY_xFe_{2-x}O_4$ nanoparticles shift towards lower 2θ values when x increases, implying that the cell constant changes and thus confirming that In^{3+} and Y^{3+} ions have entered into the structure. Table 1 lists the change of the lattice parameters. The trend towards increase of the doped zinc ferrites' lattice parameters can be understood on the basis of the ionic radii [7,8,15,16]. The cell expands with increasing x mainly as a result of the larger ionic radii of the In^{3+} (0.091 nm) and Y^{3+} ions (0.095 nm) in comparison with those of the host cations Fe^{3+} (0.067 nm) and Zn^{2+} (0.065 nm). The indium ions are known to have an initial preference for tetrahedral sites [8,9], while yttrium prefers octahedral sites [7,]. The increase of the lattice parameters, a, for the same ion concentration is more pronounced in the nanoparticles with addition of indium than with yttrium. However, it is important to note that the distribution of the cations among the tetrahedral and octahedral lattice sites of the spinel structure of nanoparticles also contributes to the changes in the lattice parameter. In fact, even for the undoped $ZnFe_2O_4$ nanoparticles the distribution of the cations over the interstitial sites influences the lattice parameter: the cell constant of the $ZnFe_2O_4$ nanoparticles is found to be 0.8452 nm, i.e. clearly larger than 0.8441 nm reported by Sickafus et al. [4] for bulk $ZnFe_2O_4$. It is well known that the finite size effects and surface effects in the nanoparticles enhance the energy of the system and consequently enable the (re)distribution of Zn^{2+} and Fe^{3+} ions [17–21]. Thus, the larger lattice parameter of the stoichiometric $ZnFe_2O_4$ nanoparticles indicate that they have a different crystal structures in terms of the cation distribution compared to the bulk material [22].

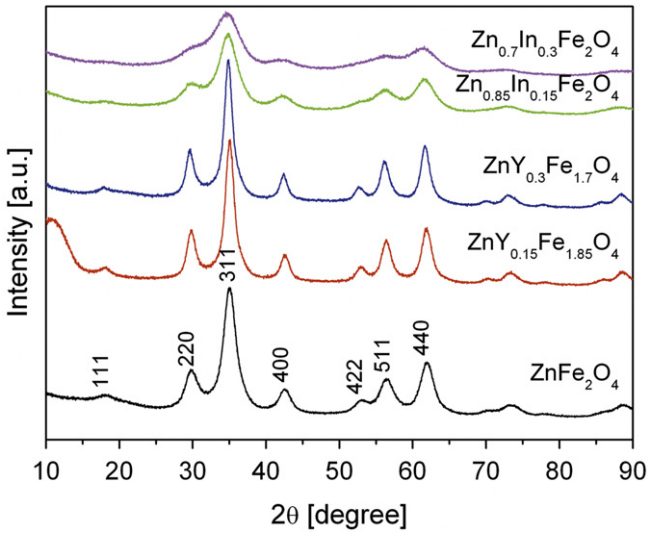

Fig. 1. XRD patterns of $Zn_{1-x}In_xFe_2O_4$ and $ZnY_xFe_{2-x}O_4$ nanoparticles.

The influence of the indium and yttrium content on the particle size was also investigated by the BET method and the results of the BET surface areas and particle sizes are shown in Table 1. These results confirm the nanostructured nature of doped samples. Increasing the indium content to 0.3 reduces the average particle size and consequently values of the specific surface area increase. In the case of the $ZnY_xFe_{2-x}O_4$ nanoparticles, the specific surface area decreases continuously with the addition of yttrium. These results are in good agreement with the XRD results. The small difference in particle size estimated from XRD and BET measurements is most likely due to nanoparticle agglomeration, which is to be expected as a result of the wet-chemistry technique used for their preparation.

Fig. 2 shows the average number size distribution of $ZnFe_2O_4$ nanoparticles. The data suggested mean particle sizes from 29 nm to 35 nm, with more than 85% of the nanoparticles to be in the range of 10–50 nm. The nanoparticle distribution fits a lognormal distribution. The average geometric mean diameter was found to be 28 ± 1.3 nm with the average standard deviation $\sigma_g = 1.59 \pm 0.01$ nm. To examine any possible structural or other changes introduced to the size of particles as a result of their treatment in an aqueous slurry, an additional test was conducted. Suspensions of variable $ZnFe_2O_4$ concentration were dispersed in liquid, such that airborne particle (aerosol) concentrations of at least one order of magnitude difference were created and the size distribution of these different particle populations was repeatedly measured. It was found that regardless of dispersion concentration, the size distributions were stable with the same standard deviation (1.6) and the geometric mean diameter showed a maximum variability of 4 nm (28–32 nm).

Table 1
Lattice constant a, specific surface area S_{BET}, average particle size estimated from XRD, d_{XRD} and average particle size estimated from BET, d_{BET} of $Zn_{1-x}In_xFe_2O_4$ and $ZnY_xFe_{2-x}O_4$ nanoparticles.

Sample	Content, x	a (nm)	S_{BET} (m^2/g)	d_{XRD} (nm)	d_{BET} (nm)
$ZnFe_2O_4$		0.845(2)	220.3	4.1	5.2
$Zn_{1-x}In_xFe_2O_4$	0.15	0.848(6)	232.6	2.9	4.8
	0.3	0.849(4)	240.4	2.2	4.5
$ZnY_xFe_{2-x}O_4$	0.15	0.846(2)	155.9	6.6	7.3
	0.3	0.847(2)	136.2	7.3	8.0

These results clearly indicate on particle agglomeration which is in accordance with the TEM results shown in Fig. 3.

According to the TEM images in Fig. 3, the as-synthesized nanoparticles are fairly uniform in size and shape. The high resolution TEM images in Fig. 3b, d and e showing the internal atomic lattice for nanocrystals and corresponding SAED patterns confirm that these nanoparticles are crystalline, having a spinel structure. The lattice fringes in Fig. 3b show an interplanar spacing of approximately 0.25 and 0.48 nm corresponding to (311) and (111) crystal planes of the spinel phase. The more defined diffraction rings of $ZnY_{0.15}Fe_{1.85}O_4$ particles, Fig. 3c, indicate that the addition of yttrium has a positive effect on particle crystallinity compared to the pure $ZnFe_2O_4$, but also in comparison to the $Zn_{0.85}In_{0.15}Fe_2O_4$ nanoparticles.

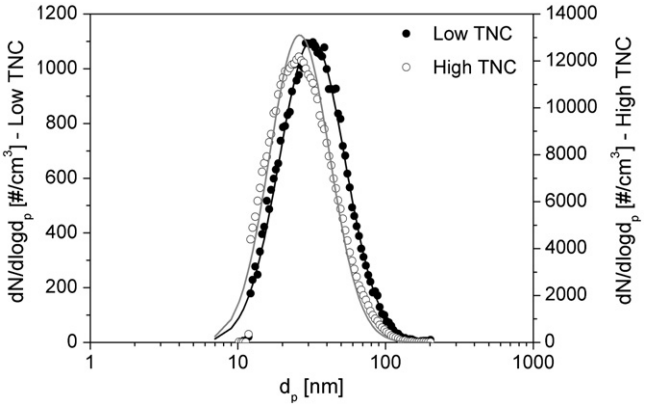

Fig. 2. Average number size distributions of $ZnFe_2O_4$ nanoparticles obtained by SMPS at low ($600\,cm^{-3}$) and high ($6000\,cm^{-3}$) suspended particles' number concentrations.

3.2. Mössbauer spectroscopy

The Mössbauer spectra of the undoped and doped zinc ferrites were recorded at $T=4.2$ K. The spectra shown in Fig. 4, could each be resolved into three well defined magnetic sextets. The fitted Mössbauer parameters i.e. magnetic hyperfine field (H), hyperfine field broadening (ΔH), isomer shift (IS), quadrupole interaction (ε), line width ($\Gamma/2$) and spectral area (A) are shown in Table 2. The presence of the six finger patterns in the spectra shows the samples to be magnetically ordered with an absence of thermal fluctuations of the magnetization at this temperature. The values of the isomer shift indicate that iron exists in the high spin Fe^{3+} valence state [11]. The values of quadrupole splitting are low indicating that the local symmetry in indium and yttrium doped ferrites is close to cubic [23–25]. The hyperfine field distributions used to fit the spectra yielded peaks located at H∼52 T and ∼49 T, with a third component at H∼46 T. In ferrites, the B–site hyperfine field is generally larger than that of the A–site, so the 52 T sextet is assigned to Fe^{3+} ions in the octahedral site and the 49 T sextet to the Fe^{3+} ions occupying the tetrahedral sites. The third sextet, H∼46 T, may also be attributed to a low field tail of octahedrally coordinated Fe^{3+} ions [23], and is designated as component B2 in Table 2. A degree of inversion in nanoparticles has been suggested as the source of the magnetic field distribution [17,26]. However, an accurate determination of the cation distribution requires the presence of an external magnetic field, where complete resolution of the overlapping subpatterns due to Fe^{3+} in A and B sites can be achieved. In any case, it is clear from the subspectral

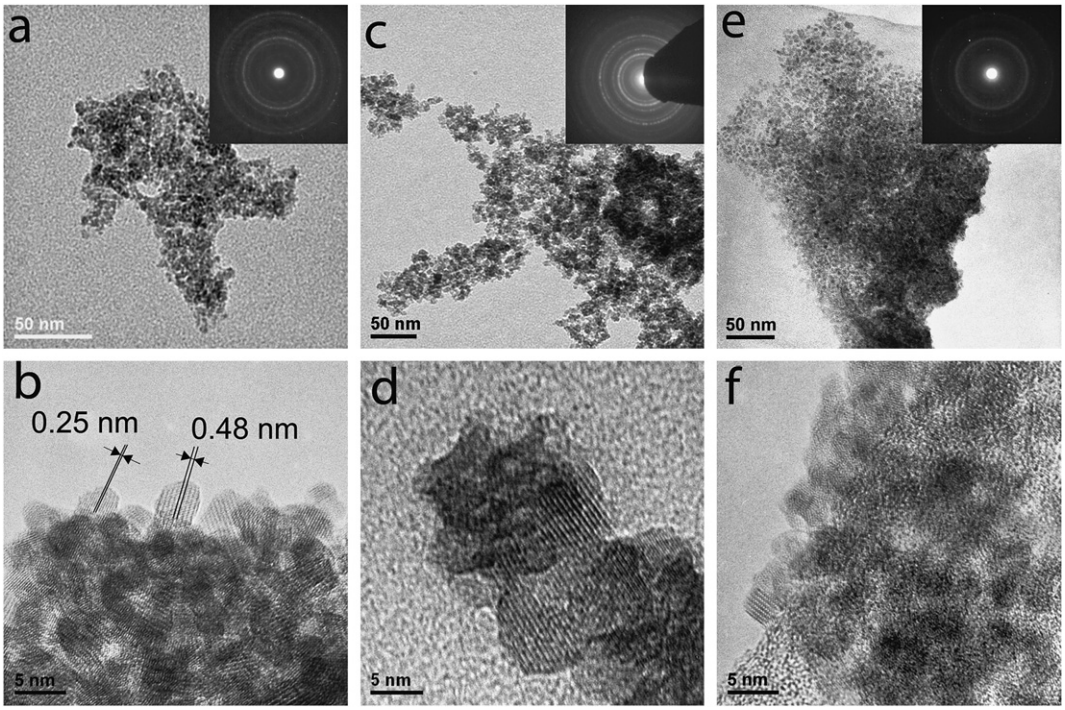

Fig. 3. TEM micrographs of nanoparticles: $ZnFe_2O_4$ (a,b), $ZnY_{0.15}Fe_{1.85}O_4$ (c,d) and $Zn_{0.85}In_{0.15}Fe_2O_4$ (e,f).

intensities, Table 2, that there is a degree of inversion in the occupancies of A and B sites, although, as previously noted, the error in the estimate of the subspectral areas is large due to the high degree of subspectral overlap. In agreement with this data, Raman measurements on the undoped and In–doped zinc ferrites [27] revealed site disorder of the Zn^{2+}, Fe^{3+} and In^{3+} ions, implying the formation of a partially inverse spinel. The doped samples, also display a degree of inversion, i.e. occupancy of the A site. The hyperfine magnetic field at both sublattices decreases in the doped samples. Since the dominant exchange interaction is the strong Fe_A^{3+}–O–Fe_B^{3+} interaction, replacing the Fe^{3+} ions with in^{3+} and Y^{3+} ions will naturally decrease the number of these interactions and consequently the hyperfine fields at both A and B sites is expected to be lowered.

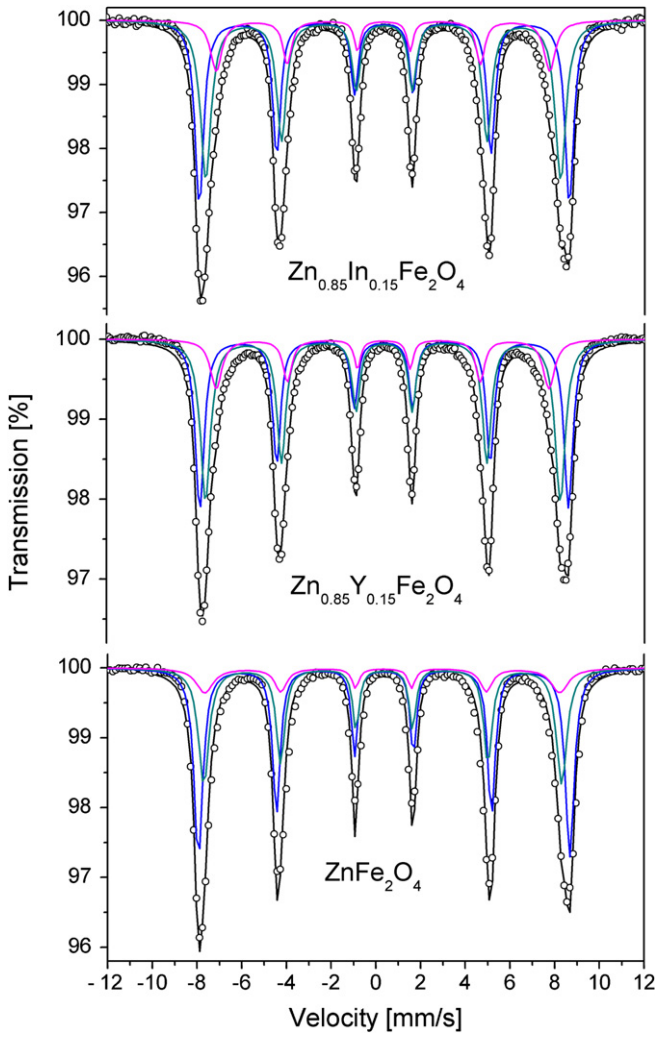

Fig. 4. Mössbauer spectra taken at $T=4.2$ K in zero field for $ZnFe_2O_4$, $ZnY_{0.15}Fe_{1.85}O_4$ and $Zn_{0.85}In_{0.15}Fe_2O_4$ nanoparticles.

3.3. Magnetization measurements

Magnetization measurements were also carried out on the samples. Fig. 5 presents the ZFC and FC magnetization as a function of temperature data. The peak in the ZFC measurements is a clear signature of superparamagnetism. In magnetic materials, nanometer dimensions lead to phenomena such as single domain nanoparticles, superparamagnetism and even enhanced magnetization (for bulk antiferromagnets or ferrimagnets). Such nanoparticles are magnetic (possessing a net moment) below a characteristic blocking temperature, T_B, and superparamagnetic above T_B. The features of the peak (i.e. width and position) and the behavior of the high-temperature tail contain useful information about the characteristics of the nanoparticles, e.g. size and size distribution [17,25]. While such information can be extracted using an assumption an non-interacting magnetic nanoparticles, even a simple comparison of the curves of different nanoparticles is very useful since it can reveal how the nanoparticles evolve as a function of an external control parameter such as doping, annealing etc.

The values of the blocking temperature of the undoped and doped zinc ferrite nanoparticles are listed in Table 3. Given that the blocking temperature refers to the temperature for which the time scale of the magnetization measurements equals the relaxation time [6,19], the anisotropy constant can be estimated from:

$$KV = k_B T_B \ln(\tau/\tau_o)$$

where K is the anisotropy constant, V is the particle volume, k_B is the Boltzmann constant, τ is the superparamagnetic

Table 2
Fitted Mössbauer parameters: Hyperfine field, H, Hyperfine field broadening ΔH, isomer shift, IS, quadrupole interaction, ε $(=e^2qQ/8)(3\cos^2\theta-1)$, linewidth, $\Gamma/2$, and spectral area, A.

Sample		H (ΔH) (T)	IS (mm/s)	ε (mm/s)	$\Gamma/2$ (mm/s)	A (%)
$ZnFe_2O_4$	A	49.9(8.0)	0.44	−0.04	0.16	37
	B1	51.8(5.0)	0.47	0.00	0.16	50
	B2	49.5(20.0)	0.42	−0.03	0.14	13
$Zn_{0.85}In_{0.15}Fe_2O_4$	A	49.4(5.0)	0.46	−0.02	0.21	44
	B1	51.5(3.0)	0.47	0.02	0.19	41
	B2	46.4(10.0)	0.44	−0.02	0.14	15
$ZnY_{0.15}Fe_{1.85}O_4$	A	49.3(5.0)	0.46	−0.03	0.2	45
	B1	51.3(3.0)	0.47	0.03	0.19	40
	B2	46.3(10.0)	0.44	−0.03	0.15	15

relaxation time and τ_o is a relaxation time factor, $\tau_o \sim 10^{-10}$ s. A value of $K = 2.7 \cdot 10^6$ erg/cm^3 was obtained for the as-synthesized $ZnFe_2O_4$ nanoparticles, Table 3, which is in good accordance with the literature data [19,28].

The field dependences of the $Zn_{1-x}In_xFe_2O_4$ and $ZnY_xFe_{2-x}O_4$ nanoparticles' magnetization at 5 K and 300 K are shown in Figs. 6 and 7. All the samples show hysteresis at 5 K, which completely vanishes at 300 K. Magnetization measurements at room temperature show that the magnetization does not fully saturate even at the highest applied field of 5 T implying the presence of single domain nanoparticles in the superparamagnetic state, while the hysteresis and unsaturated magnetization imply blocking of the ferrimagnetic nanoparticles at 5 K [29]. The magnetization of spinel ferrites originates from the difference in the net magnetic moment of the ions at the octahedral and at the tetrahedral lattice sites. According to Neel model, A−B superexchange interactions are predominant over intrasublattice A−A and B−B interactions, and the saturation magnetization is given by the vector sum of the net magnetic moments of the individual A and B sublattices [7–9]. Since Zn^{2+}, In^{3+} and Y^{3+} ions are non−magnetic they do not contribute to the overall magnetization. So, the magnetization directly reflects the distribution of the magnetic Fe^{3+} between the two sublattices. If the magnetic Fe^{3+} ions occupy both tetrahedral and octahedral sites, this will result in ferrimagnetic ordering. We found that all the samples exhibited ferrimagnetism. The value of the saturation magnetization for $ZnFe_2O_4$ nanoparticles is about 63.2 emu/g at $T = 5$ K, which is higher than the reported value of ~5 emu/g for bulk $ZnFe_2O_4$ [17,30]. The most likely source of such large magnetization in nanoparticles over bulk is the cation redistribution and the formation of a partially inversed spinel. The location of Fe^{3+} ions on tetrahedral sites results in Fe_A^{3+}–O–Fe_B^{3+} superexchange interactions and causes the magnetization to increase drastically. This is in accordance with previous results.

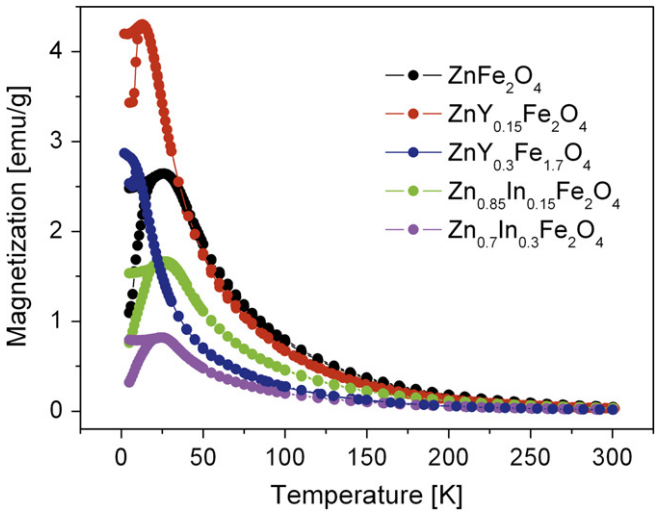

Fig. 5. Zero−field cooled (ZFC) and field cooled (FC) magnetization temperature dependence of $Zn_{1-x}In_xFe_2O_4$ and $ZnY_xFe_{2-x}O_4$ nanoparticles obtained with an applied field of 100 Oe.

The nanoparticles' magnetic properties change with their composition, Table 3. Addition of indium into zinc ferrite nanoparticles results in an increase of the coercivity, H_c and in a decrease of the saturation magnetization, M_s, Fig. 6. The larger values of coercivity for the $Zn_{1-x}In_xFe_2O_4$ nanoparticles indicate a higher degree of disorder compared to the $ZnFe_2O_4$ nanoparticles. The decrease of saturation magnetization implies that addition of indium causes structural rearrangements (resulting in decreased number of Fe_A^{3+}–O–Fe_B^{3+} interactions) and/or magnetic dilution (in the case that indium substitutes not only zinc but iron as well). The observed reduction of the saturation magnetization and the high-field magnetization irreversibility in ferrimagnetic nanoparticles has renewed interest in these systems. Spin canting, defined as a lack of full alignment of the spins in magnetic particles has usually been proposed to account for these observations [31–34]. In addition, for such fine nanoparticles ($d < 4$ nm), surface effects can be dominant; with surface spins responsible for decrease in the magnetization [6]. In general as the particle size decreases surface effects become increasingly important [17,18]. Broken bonds and asymmetric environment of the surface layers will lead to noncollinear spin arrangement at the surface. In the case of smaller particles the increased surface to volume ratio creates crystallographic strains and distortions close to the surface. These strains can increase the anisotropy of the particle, which is observed in the indium doped zinc ferrite nanoparticles, Table 3.

Magnetic measurements of yttrium doped zinc ferrite nanoparticles, similar to the In-doped system, showed them to be ferrimagnetic with some degree of

Table 3
Blocking temperature, T_B anisotropy constant, K and corecive field, H_c of $Zn_{1-x}In_xFe_2O_4$ and $ZnY_xFe_{2-x}O_4$ nanoparticles at $T = 5$K. Saturation magnetizations, M_s were obtained by by extrapolating the high-field M(1/H) experimental data to 1/H = 0.

Sample	Content, x	T_B (K)	H_c (Oe)	K (erg/cm^3)	M_s, 5 K (emu/g)	M_s, 300 K (emu/g)
$ZnFe_2O_4$		26	204.6	2.7×10^6	63.2	22.9
$Zn_{1-x}In_xFe_2O_4$	0.15	27	301.4	0.81×10^7	48.2	16.5
	0.3	25	364.7	1.71×10^7	37.9	12.1
$ZnY_xFe_{2-x}O_4$	0.15	13	75.7	3.3×10^5	66.5	22.4
	0.3	9	57	1.7×10^5	50.4	20.1

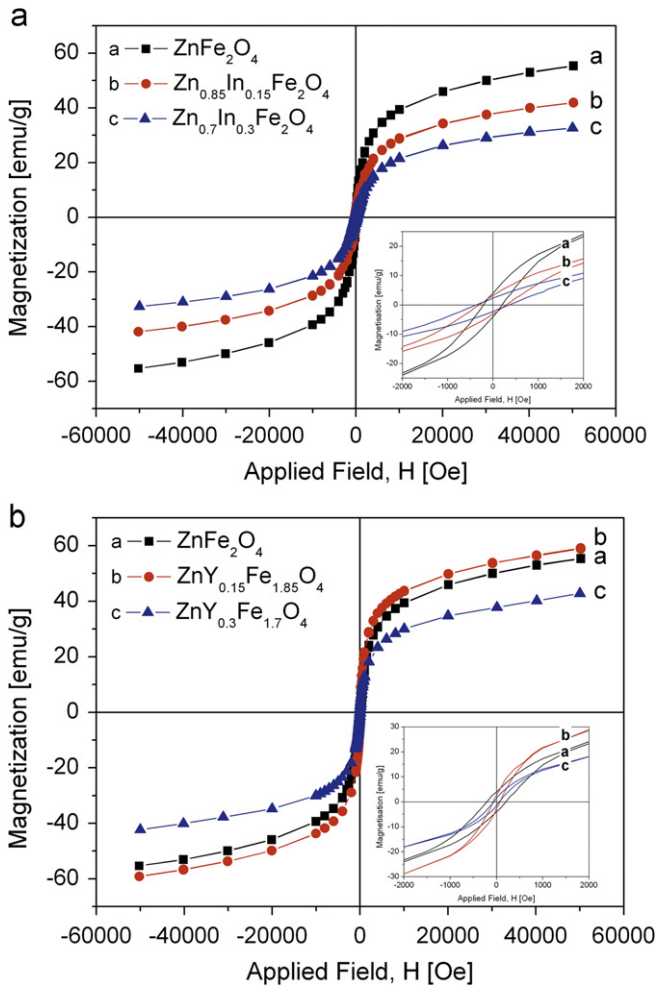

Fig. 6. Magnetization versus applied magnetic field at $T=5$ K for: (a) $Zn_{1-x}In_xFe_2O_4$ and (b) $ZnY_xFe_{2-x}O_4$ nanoparticles. Inset shows the variation at lower applied fields.

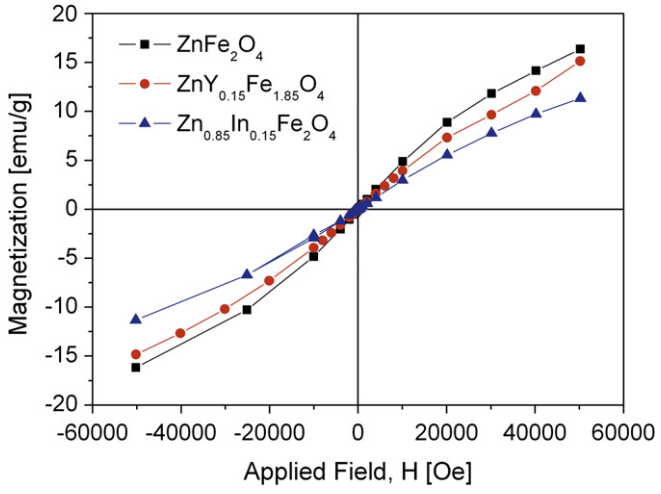

Fig. 7. Magnetization versus applied magnetic field at $T=300$ K.

noncollinearity of the surface spins. Yttrium doped zinc ferrites have higher values of saturation magnetization in comparison to the indium doped. Whereas the addition of indium leads to particle size reduction, significant surface effects, lattice strain and a high degree of disorder, the addition of yttrium promotes the energetically favored ordered structure. This is clear primarily from a consideration of ZFC-FC magnetization curves, where an obvious decrease of the blocking temperature with the addition of yttrium can be seen, Table 3. As the blocking temperature approaches the Neel temperature of the normal $ZnFe_2O_4$ spinel $T_N=10$ K, it can be assumed that yttrium stabilizes Fe^{3+} ions in the octahedral sites, thus reducing the tendency towards inversion. By stabilizing the Fe^{3+} in octahedral sites, the structure becomes closer to the ordered, which is characterized by a minimum of stress. This is in accordance with the calculated anisotropy constants for the yttrium doped nanoparticles which are one order of magnitude less than that of nanocrystalline $ZnFe_2O_4$, Table 4. The values of coercivity observed for the yttrium doped zinc ferrites are quite low ($H_c<75$ Oe) in comparison with those of the undoped and indium doped. Thus the addition of yttrium results in magnetically soft ferrites.

4. Conclusion

Nanoparticles of indium and yttrium doped zinc ferrite were successfully synthesized using a co-precipitation method. Structural analysis has shown that the single phase spinel ferrites with sizes of a few nanometers are formed in all samples. While the as-prepared nanoparticles are superparamagnetic at room temperature, they show ferrimagnetic behavior at low temperatures. Saturation magnetization of the investigated nanoparticles decreases with increasing concentration of dopants indicating a lowering of the number of Fe_A^{3+}–O–Fe_B^{3+} superexchange interactions. Increasing indium concentration leads to a particle size reduction causing pronounced surface effects. As a result of the large lattice strain, the anisotropy constant and the coercive field increase. In contrast, the addition of yttrium results in larger particles lowering the lattice strain in accordance with the calculated anisotropy constants, which are one order of magnitude smaller than those of the undoped zinc ferrites. The Mössbauer measurements showed well defined magnetic sextets assigned to the tetrahedral and octahedral sites implying some degree of inversion with occupancy of A and B sites by the Fe^{3+} cations.

Acknowledgment

Authors would like to acknowledge the support from the Ministry of Education, Science and Technological Development, Republic of Serbia, Project "Synthesis of nanopowders and processing of ceramics and nanocomposites with specific electric and magnetic properties for application in integrated passive components", no. III45021. E.G.M. acknowledges support from the COST Action SIMUFER. She also thanks the Research Funding Program Thalis which is co-financed by the European Union (European Social Fund; ESF) and Greek national funds through the Operational Program

"Education and Lifelong Learning" of the National Strategic Reference Framework (NSRF)".

References

[1] R. Raeisi Shahraki, M. Ebrahimi, S.A. Seyyed Ebrahimi, S.M. Masoudpanah, Structural characterization and magnetic properties of superparamagnetic zinc ferrite nanoparticles synthesized by the coprecipitation method, Journal of Magnetism and Magnetic Materials 324 (2012) 3762–3765.

[2] T.J. Shinde, A.B. Gadkari, P.N. Vasambekar, Effect of Nd^{3+} substitution on structural and electrical properties of nanocrystalline zinc ferrite, Journal of Magnetism and Magnetic Materials 322 (2010) 2777–2781.

[3] R. Sai, S.D. Kulkarni, K.J. Vinoy, N. Bhat, S.A. Shivashankar, $ZnFe_2O_4$: rapid and sub–100 °C synthesis and anneal-tuned magnetic properties, Journal of Materials Chemistry 22 (2012) 2149–2156.

[4] K.E. Sickafus, J.M. Wills, N.W. Grimes, Structure of spinel, Journal of the American Ceramic Society 82 (1999) 3279–3292.

[5] M. Mozaffari, M. Eghbali Arani, J. Amighian, The effect of cation distribution on magnetization of $ZnFe_2O_4$ nanoparticles, Journal of Magnetism and Magnetic Materials 322 (2010) 3240–3244.

[6] V. Blanco–Gutierrez, E. Climent–Pascual, M.J. Torralvo–Fernandez, R. Saez–Puche, M.T. Fernandez–Diaz, Neutron diffraction study and superparamagnetic behavior of $ZnFe_2O_4$ nanoparticles obtained with different conditions, Journal of Solid State Chemistry 184 (2011) 1608–1613.

[7] Q. Xing, Z. Peng, C. Wang, Z. Fu, X. Fu, Doping effect of Y^{3+} ions on the microstructural and electromagnetic properties of Mn–Zn ferrites, Physica B 407 (2012) 388–392.

[8] S.E. Shirsath, B.G. Toksha, K.M. Jadhav, Structural and magnetic properties of In^{3+} substituted $NiFe_2O_4$, Materials Chemistry and Physics 117 (2009) 163–168.

[9] S. Verma, J. Chand, M. Singh, Effect of In^{3+} ions doping on the structural and magnetic properties of $Mg_{0.2}Mn_{0.5}Ni_{0.3}In_xFe_{2-x}O_4$ spinel ferrites, Journal of Magnetism and Magnetic Materials 324 (2012) 3252–3260.

[10] Z. Cvejić, S. Rakić, S. Jankov, S. Skuban, A. Kapor, Dielectric properties and conductivity of zinc ferrite and zinc ferrite doped with yttrium, Journal of Alloys and Compounds 480 (2009) 241–245.

[11] M. Hashim Alimuddin, S. Kumar, S.E. Shirsath, R.K. Kotnala, H. Chung, R. Kumar, Structural properties and magnetic interactions in $Ni_{0.5}Mg_{0.5}Fe_{2-x}Cr_xO_4$ $(0 \le x \le 1)$ ferrite nanoparticles, Powder Technology 229 (2012) 37–44.

[12] G. Stojanović, V. Srdić, M. Maletin, Electrical properties of yttrium-doped Zn and Ni–Zn ferrites, Physica Status Solidi A 205 (10) (2008) 2464–2468.

[13] M. Maletin, E.G. Moshopoulou, S. Jankov, S. Rakić, V.V. Srdić, The effect of yttrium and indium doping on the structure and electrical properties of zinc-ferrite nanoparticles, Solid State Phenomena 128 (2007) 101–105.

[14] D.B. Cullity, in: Elements of X–ray Diffraction, 2nd Ed., Addison-Wesley Publishing Company, Reading, Massachusetts, 1977.

[15] B.P. Rao, K.H. Rao, Distribution of In^{3+} ions in indium–substituted Ni–Zn–Ti ferrites, Journal of Magnetism and Magnetic Materials 292 (2005) 44–48.

[16] M. Ishaque, M.U. Islam, M. Azhar Khan, I.Z. Rahman, A. Genson, S. Hampshire, Structural, electrical and dielectric properties of yttrium substituted nickel ferrites, Physica B 405 (2010) 1532–1540.

[17] C.N. Chinnasamy, A. Narayanasamy, N. Ponpandian, K. Chattopadhyay, H. Guérault, J.–M. Greneche, Magnetic properties of nanostructured ferrimagnetic zinc ferrite, Journal of Physics Condensed Matter 12 (2000) 7795–7805.

[18] M. Atif, S.K. Hasanain, M. Nadeem, Magnetization of sol–gel prepared zinc ferrite nanoparticles: effects of inversion and particle size, Solid State Communications 138 (2006) 416–421.

[19] C. Yao, Q. Zeng, G.F. Goya, T. Torres, J. Liu, H. Wu, M. Ge, Y. Zeng, Y. Wang, J.Z. Jiang, $ZnFe_2O_4$ nanocrystals: synthesis and magnetic properties, Journal of Physical Chemistry C 111 (2007) 12274–12278.

[20] J. Philip, G. Gnanaprakash, G. Panneerselvam, M.P. Antony, T. Jayakumar, B. Raj, Effect of thermal annealing under vacuum on the crystal structure, size, and magnetic properties of $ZnFe_2O_4$ nanoparticles, Journal of Applied Physics 102 (2007) 054305.

[21] A.E. Berkowitz, R.H. Kodama, S.A. Makhlouf, F.T. Parker, F.E. Spada, E.J. McNiff Jr., S. Foner, Anomalous properties of magnetic nanoparticles, Journal of Magnetism and Magnetic Materials 196–197 (1999) 591–594.

[22] D. Makovec, A. Kodre, I. Arcon, M. Drofenik, Structure of manganese zinc ferrite spinel nanoparticles prepared with co–precipitation in reversed microemulsions, Journal of Nanoparticle Research 11 (2009) 1145–1158.

[23] S. Verma, P.A. Joy, S. Kurian, Structural, magnetic and Mössbauer spectral studies of nanocrystalline $Ni_{0.5}Zn_{0.5}Fe_2O_4$ ferrite powders, Journal of Alloys and Compounds 509 (2011) 8999–9004.

[24] M. Gupta, B.S. Randhawa, Mössbauer, magnetic and electric studies on mixed Rb–Zn ferrites prepared by solution combustion method, Materials Chemistry and Physics 130 (2011) 513–518.

[25] I. Soibam, S. Phanjoubam, C. Prakash, Mössbauer and magnetic studies of cobalt substituted lithium zinc ferrites prepared by citrate precursor method, Journal of Alloys and Compounds 475 (2009) 328–331.

[26] V. Sepelak, I. Bergmann, S. Kipp, K.D. Becker, Nanocrystalline ferrites prepared by mechanical activation and mechanosynthesis, Zeitschrift Fur Anorganische Und Allgemeine Chemie 631 (2005) 993–1003.

[27] M. Maletin, E.G. Moshopoulou, A.G. Kontos, E. Devlin, A. Delimitis, V.T. Zaspalis, L. Nalbandian, V.V. Srdic, Synthesis and structural characterization of In-doped $ZnFe_2O_4$ nanoparticles, Journal of the European Ceramic Society 27 (2007) 4391–4394.

[28] A.T. Ngo, P. Bonville, M.P. Pileni, Spin canting and size effects in nanoparticles of nonstoichiometric cobalt ferrite, Journal of Applied Physics 89 (2001) 3370.

[29] C. Upadhyay, H.C. Verma, V. Sathe, A.V. Pimpale, Effect of size and synthesis route on the magnetic properties of chemically prepared nanosize $ZnFe_2O_4$, Journal of Magnetism and Magnetic Materials 312 (2007) 271–279.

[30] M.R. Anantharaman, S. Jagatheesan, K.A. Malini, S. Sindhu, A. Narayanasamy, C.N. Chinnasamy, J.P. Jacobs, S. Reijne, K. Seshan, R.H.H. Smits, H.H. Brongersma, On the magnetic properties of ultra-fine zinc ferrites, Journal of Magnetism and Magnetic Materials 189 (1998) 83–88.

[31] R.H. Kodama, A.E. Berkowitz, E.J. McNiff, S. Foner, Surface spin disorder in ferrite nanoparticles, Journal of Applied Physics 81 (1997) 5552.

[32] R.D.K. Misra, S. Gubbala, A. Kale, W.F. Egelhoff Jr., A comparison of the magnetic characteristics of nanocrystalline nickel, zinc, and manganese ferrites synthesized by reverse micelle technique, Materials Science and Engineering B 111 (2004) 164–174.

[33] G. Vaidyanathan, S. Sendhilnathan, Characterization of $Co_{1-x}Zn_x$-Fe_2O_4 nanoparticles synthesized by co-precipitation method, Physica B 403 (2008) 2157–2167.

[34] Z. Zi, Y. Sun, X. Zhu, Z. Yang, J. Dai, W. Song, Synthesis and magnetic properties of $CoFe_2O_4$ ferrite nanoparticles, Journal of Magnetism and Magnetic Materials 321 (2009) 1251–1255.